Inorganica Chimica Acta 578 (2025) 122537

Contents lists available at ScienceDirect

Inorganica Chimica Acta

journal homepage: www.elsevier.com/locate/ica

Research paper

Polypyridyl Os(II) complexes as efficient human non-small cell lung cancer photosensitizers with enhanced singlet oxygen generation *via* the fused π-ring elongation

Feng Chen [a,*], Kelun Cui [a], Shufen Si [b], Yong Liu [a], Songlin Xue [a], Gaoji Wang [a], Xu Liang [a,*], Chunyin Zhu [a], Qiu-Yun Chen [a,*]

[a] School of Chemistry and Chemical Engineering, Jiangsu University, Zhenjiang 212013 PR China
[b] Northern Light Quality Inspection Technical Service Co., Ltd., Nanjing 210033 PR China

ARTICLE INFO

Keywords:
Polypyridyl osmium complex
Singlet oxygen
Photosensitizer
Antiproliferative activity

ABSTRACT

Photodynamic therapy as a complementary cancer treatment strategy has attracted rising interests. Here, five polypyridyl Os(II) complexes **Os-1** − **Os-5** with the general formula of $[(DIP)_2OsL](PF_6)_2$ have been synthesized and fully characterized by $^1H/^{13}C$ NMR, HRMS and elemental analysis. Their electronic properties were studied by electrochemistry, and DFT and TD-DFT calculations. A significant enhancement of singlet oxygen ($^1O_2$) generation was observed with π extension on the coordinative ligands, that **Os-3** with dibenzo[*a*,*c*]dipyrido[3,2-h:2′,3′-j]phenazine ligand showed the highest induction capacity under blue LED light (465 nm in acetonitrile), with the quantum yield ($\Phi_{\Delta S}$) of 0.65 in comparison to that of $[(bpy)_3RuCl_2]$ ($\Phi_{\Delta(S0)}$, 0.57); **Os-3** remained the highest $^1O_2$ generation ability under red LED irradiation (640 nm). All complexes showed potent photocytotoxicity against MGC-803 and HGC-27 human gastric cancer cells, giving IC_{50} value low as 0.37 μM (blue LED light) and 0.32 μM (blue LED light), and PI value was high as 15 in A549 cancer cells inhibition. The cellular $^1O_2$ detection by SOSG showed a concentration-dependent manner when co-administered with **Os-3** in HGC-27 cells, and the absorbed Os content was up to 96.1 ng/10^6 cells in A549 cells for **Os-3**. Subcellular colocalization indicated that those Os(II) complexes are less likely targeting mitochondria. Together, the enhancement of $^1O_2$ generation by ligand modification may provide a feasible strategy for the design of new photosensitizers, and such type of Os(II) complexes have the potential application as new human gastric cancer photosensitizers.

1. Introduction

To date, cisplatin and its analogs carboplatin or oxaliplatin are still in routine use in chemo-therapy for various cancers treatment [1]; the success but intrinsically attached defects of cisplatin or other platinum-based chemotherapeutic drugs have aroused and flourished the intensive antiproliferative investigation on other platinum group transition metals for the last two decades, *e.g.* Ru(II) [2,3], Ir(III) [4,5,6], Re(I) [7,8], and Au(III) [9], and more importantly, the photodynamic therapy.

Photodynamic therapy (PDT), with noninvasive and high selective qualities, has emerged as a prominent complementary process to platinum-based chemotherapy for the treatment of cancers or other diseases [10]. The clinical use of porphyrin-based molecules as the first generation of photosensitizers (PSs), for instance Photofrin and Protoporphyrin IX (PpIX), could retrospect to last 90 s [10]. In comparison to the traditional porphyrin PSs, transition-metal included PSs possessed several apparent advantages, like adjustable and longer emission, higher emissive quantum yields, larger Stoke shift, photobleaching resistance, *etc* [10,11]; thus are promising photosensitizer candidates for next generation of PSs for cancer treatment. So far, great efforts for development of transition-metal based PSs, exemplarily, TLD-1433, a Ru(II) PS for curing non-muscle invasive bladder cancer [12], and WST11, a Pd (II) derivative as bacteriopheophorbide [13], have been achieved. Mechanically, PS is evoked from the ground state to an excited singlet state under an irradiative excitation, and undergo an intersystem crossing (ISC) process to the triplet state. Subsequently it can decay to the ground state by the luminescence emission through two pathways, i.e., type I, which typically generate reactive oxygen species, *e.g.*, $O_2^{\cdot-}$ and $OH^{\cdot}$, by water or biomolecules oxidation (electron transfer in mechanism); and type II, majorly induces singlet oxygen ($^1O_2$) generation (excited energy

* Corresponding authors.
E-mail address: fengjchen@ujs.edu.cn (F. Chen).

https://doi.org/10.1016/j.ica.2025.122537
Received 4 November 2024; Received in revised form 1 January 2025; Accepted 1 January 2025
Available online 3 January 2025

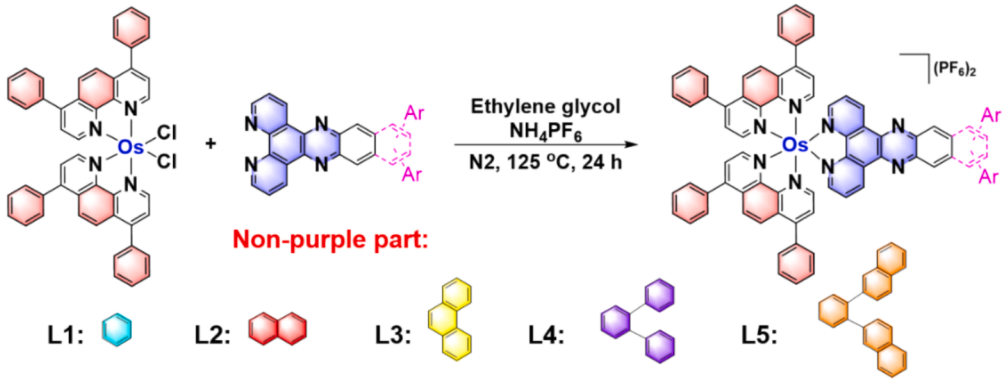

Scheme 1. Illustrated synthesis route of Os-1 – Os-5.

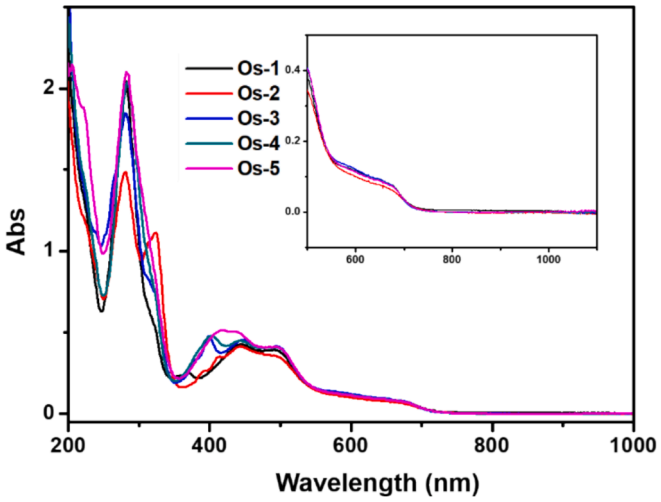

Fig. 1. UV–vis spectra of complexes Os-1 – Os-5 in acetonitrile; inset is absorbance of Os-1 – Os-5 in 500–1000 nm range.

transfer in mechanism) [14,15]. The property of $^1O_2$, for example short lifetime (< 3 μs) and low diffusion distance (2–4 × 10^6 cm^2 s^{-1}), endowed PDT with highly regionalized quality [16]. Many transition-metal based PSs can generate sufficient singlet oxygen [11,17]; among those, Ru(II) complexes undoubtedly are the most investigated PSs in PDT [18,19]. However, low oxygen concentration and minimal light penetration have enormously limited their further *in vivo* application. Benefiting from the significant heavier metal effect, the analogous Os(II) complexes which were far less developed and studied [20], might show an significant red-shift up to a deep red to near inferred region in comparison to the respective Ru(II) complexes. The possible 'biological window' (700–1000 nm) localization and excitation for Os(II) complexes led to an optimal light penetration and more practical application targeting deeper tissual solid tumors [21]. Furthermore, the characteristic full absorbance and longer excited-state lifetime provoke better sensitivity to trace amount of oxygen for Os(II) complexes [22]. McFarland and coworkers have developed a series of panchromatic Os (II) polypyridyl PSs derived from the scaffold of TLD-1433, i.e. TLD1822, TLD1824 and TLD1829, have shown potent PDT efficacy under both red and near-infrared light in normoxic and hypoxic conditions [23]. Gasser and Chao *et al.* synthesized various structurally simple but hypoxically active osmium(II) polypyridyl complexes, $[Os(4,7\text{-diphenyl-1,10-phenanthroline})_2L]^{2+}$, with $^1O_2$ quantum as high as 0.415, these complexes have shown promising phototoxicity in 2D cell layers and multicellular tumor spheroids, as well as on CT26 tumor-bearing BALB/c mice upon NIR irradiation [24]. Zhang *et al.* reported an osmium-peroxo complex that can release a peroxo ligand $O_2^{\bullet-}$ upon light irradiation even in the absence of oxygen, such complex induced photocatalytic oxidation of endogenous 1,4-dihydronicotinamide adenine dinucleotide, leading to ferroptosis, that is mediated by glutathione degradation, lipid peroxide accumulation in living cells [25].

Nevertheless, unsatisfactory amount of $^1O_2$ was inductively obtained for many complexes due to the more sophisticated conditions [21,26], like low ISC efficiency or the fast nonradiative deactivation process by intramolecular vibrational relaxation [27,28]. Accordingly, rational design, for instance complex with rigid molecular structure, is required to reduce the vibrational relaxation rate [29,30], thus may will facilitate the enhancement of $^1O_2$ quantum yield; other strategies to modulate the $^1O_2$ production, *e.g.* plasmonic nanoparticles [31,32], aggregates [33], or FRET strategy [34], etc, were also endeavored, to boost the $^1O_2$ generation. Capitalized on this, we seek to design and synthesize a series of Os(II)-based photosensitizers having potent $^1O_2$ generation capacity, and to study the structure–activity-relationship. In current work, five Os (II) polypyridyl complexes with the general formula of $[(DIP)_2OsL](PF_6)_2$, where DIP is 4,7-diphenyl-1,10-phenanthroline, and L are dipyrido[3,2-*a*:2′,3′-*c*]phenazine(dppz, L1), benzo[*i*]dipyrido[3,2-*a*:2′,3′-*c*]phenazine (dppn, L2), dibenzo[*a*,*c*]dipyrido[3,2-h:2′,3′-j]phenazine(dppp, L3), 11,12-diphenyldipyrido[3,2-*a*:2′,3′-*c*]phenazine (dppzb, L4), 11,12-di(naphthalen-2-yl)dipyrido[3,2-*a*:2′,3′-*c*]phenazine (dppzn, L5), have been synthesized and characterized. CV and DFT/TD-DFT calculations were performed to study the electronic property. The $^1O_2$ generation capacity by **Os-1** – **Os-5** under blue and red LED lights irradiation was also determined. *In vitro* antiproliferative activity against three human cancer cell lines, *i.e.*, A549 human non-small cell lung cancer, MGC-803, and HGC-27 (undifferentiated) human gastric cancer cells was also investigated. The cellular $^1O_2$ generation, cell uptake, and subcellular colocalization were studied as well.

2. Materials and experimental section

All solvents (reagent grade) were obtained from commercial resources, and used without further purification. Ammonium hexachloroosmate(IV) was purchased from Xiya Reagent Chemical Co., Ltd (Shandong, China); 1,10-phenanthroline-5,6-dione, 2,3-diaminonaphthalene, phenanthrene-9,10-diamine, 4,5-dibromo-1,2-phenylenediamine and tetrakis(triphenyl phosphine)palladium were purchased from Leyan Chemical Co., Ltd (Shanghai, China); 2-naphthaleneboronic acid was obtained from Macklin Biochemical Technology Co., Ltd (Shanghai, China); 4,7-diphenyl-1,10-phenanthroline (DIP) was obtained from Titan Technology Co., Ltd (Shanghai, China). 9,10-anthracenediyl-bis-(methylene) dimalonic acid (ABDA) and 1,3-Diphenylisobenzofuran (DPBF) were obtained from Admas. ^1H- and ^{13}C NMR spectra were recorded on a JNM-ECX 400 MHz NMR spectrometer. UV – vis spectra were measured on a UV-3600 Plus spectrometer (Tokyo, Japan).

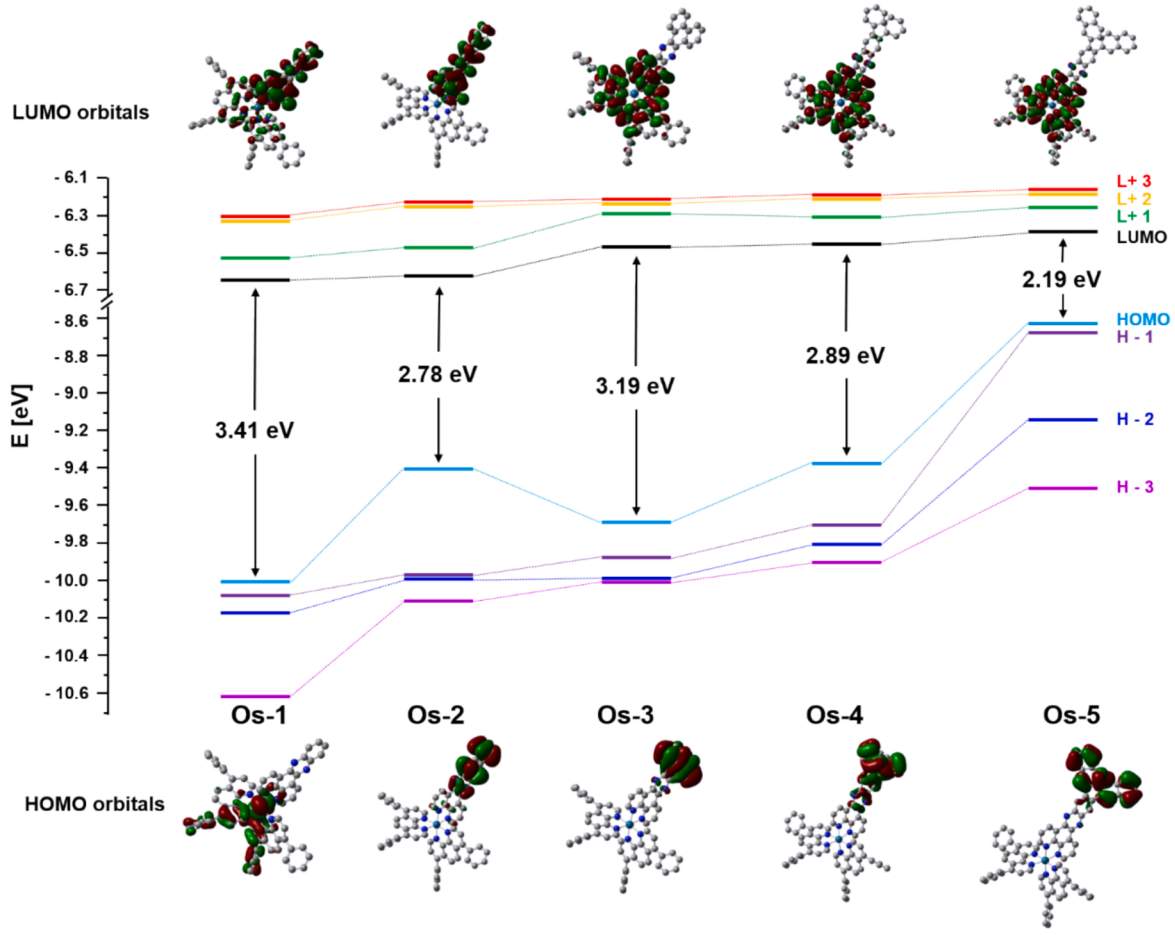

Fig. 2. Diagram of molecular orbital energy level with the electron density of the HUMO and LUMO for complexes Os-1 – Os-5.

3. Instruments and basic methods

3.1. Synthesis and characterization

The chelated ligands of dipyrido[3,2-*a*:2′,3′-*c*]phenazine(dppz, L1) [35], benzo[i]- dipyrido[3,2-*a*:2′,3′-*c*]phenazine (dppn, L2) [36], dibenzo[*a*,*c*]dipyrido[3,2-h:2′,3′-j]phenazine(dppp, L3) [37], 11,12-diphenyldipyrido[3,2-*a*:2′,3′-*c*]phenazine(dppzb, L4) and 11,12-di(naphthalen-2-yl)dipyrido[3,2-*a*:2′,3′-*c*]phenazine(dppzn, L5) [38] were obtained according to the reported synthetic procedures. The osmium (II) precursor $Os(DIP)_2Cl_2$ were synthesized according to the reported method [24,39].

All Os(II) complexes were synthesized according an established procedure [24]. In general, to a solution of $[Os(DIP)_2Cl_2]$ (1 eq.) in degassed ethylene glycol (20 mL) was added the coordinative ligands (1.1 eq.). The mixture was heated at 125 °C under N_2 for 24 h. After the solution was cooling to room temperature, a saturated aqueous solution of ammonium hexafluorophosphate (10 mL) was added, and the dark brown precipitate was immediately formed; the solid was obtained by filtration, washed with deionized water (25 mL × 3) and diethyl ether (25 mL × 3). The crude product was then purified by silica column chromatography (DCM/MeOH, 30:1) and preparative thin layer chromatography (DCM/MeOH, 35:1), with black-purple solids were obtained.

Os-1 $[(DIP)_2Os(dppz)](PF_6)_2$. Yield: 273 mg, 53 %. ^{1}H NMR (400 MHz, $CDCl_3$) δ_H 7.51–7.66 (m, 20H), 7.73 (d, J = 4 Hz, 2H), 7.78 (d, J = 4 Hz, 2H), 7.91 (d, J = 4 Hz, 2H), 8.06 (d, J = 4 Hz, 2H), 8.26 (d, J = 4 Hz, 4H), 8.30–8.43 (m, 8H), 9.42 (s, 2H); ^{13}C NMR (100 MHz, $CDCl_3$) δ_C 152.7, 152.2, 151.3, 149.9, 149.8, 149.1, 148.9, 142.6, 139.2, 134.7, 132.1, 130.7, 129.7, 129.4, 128.9, 128.7, 127.9, 126.7, 126.6, 126.3, 126.2; HRMS-$[M]^{2+}$ Found: 569.1575 *m/z*, calculated: 569.1574 *m/z*. Anal. Calcd for $[C_{66}H_{42}F_{12}N_8OsP_2]$: C, 55.54; H, 2.97; N, 7.85. Found: C, 55.67; H, 3.12; N, 7.79.

Os-2 $[(DIP)_2Os(dppn)](PF_6)_2$. Yield: 318 mg, 60 %.^{1}H NMR (400 MHz, $CDCl_3$) δ_H 7.50–7.69 (m, 22H), 7.75–7.79 (m, 6H), 8.15–8.19 (m, 2H), 8.27 (d, J = 12 Hz, 4H), 8.32 (d, J = 4 Hz, 2H), 8.43 (d, J = 8 Hz, 2H), 8.84–8.88 (m, 2H), 8.15–8.21 (m, 2H); ^{13}C NMR (100 MHz, $CDCl_3$) δ_C 152.9, 152.8, 151.6, 151.5, 150.1, 150.0, 149.8, 149.2, 148.9, 135.0, 134.8, 132.9, 130.8, 129.9, 129.8, 129.5, 129.0, 128.9, 128.8, 128.4, 128.1, 128.0, 127.9, 126.9, 126.4, 126.2; HRMS-$[M]^{2+}$ Found: 594.1652 *m/z*, calculated: 594.1652 *m/z*. Anal. Calcd for $[C_{70}H_{44}F_{12}N_8OsP_2(H_2O)_{0.4}]$: C, 56.63; H, 3.04; N, 7.55. Found: C, 56.68; H, 3.32; N, 7.58.

Os-3 $[(DIP)_2Os(dppp)](PF_6)_2$. Yield: 228 mg, 42 %.^{1}H NMR (400 MHz, d_6-DMSO) δ_H 7.67–7.70 (m, 8H), 7.72–7.75 (m, 12H), 7.79 (d, J = 8 Hz, 2H), 7.83 (dd, J_1 = 8 Hz, J_2 = 8 Hz, 4H), 7.79–8.05 (m, 4H), 8.31–8.40 (m, 10*H*), 8.96 (d, J = 8 Hz, 2H), 9.65 (d, J = 8 Hz, 2H), 9.80 (d, J = 8 Hz, 2H); ^{13}C NMR (100 MHz, d_6-DMSO) δ_C 152.1, 150.1, 147.9, 147.8, 147.7, 141.5, 138.5, 135.2, 135.1, 131.9, 131.4, 130.2, 130.1, 129.7, 129.2, 128.8, 128.5, 128.3, 127.9, 126.7, 126.3, HRMS-$[M]^{2+}$ Found: 619.1729 *m/z*, calculated: 619.1730 *m/z*. Anal. Calcd for $[C_{74}H_{46}F_{12}N_8OsP_2(H_2O)_{2.2}]$: C, 56.72; H, 3.24; N, 7.15. Found: C, 56.71; H, 3.40; N, 7.18.

Os-4 $[(DIP)_2Os(dppzb)](PF_6)_2$. Yield: 347 mg, 62 %. ^{1}H NMR (400 MHz, $CDCl_3$) δ_H 7.19–7.25 (m, 5H), 7.32 (d, J = 4 Hz, 2H), 7.51–7.60 (m, 16H), 7.63–7.68 (m, 6H), 7.76 (d, J = 8 Hz, 3H), 7.79 (d, J = 4 Hz, 2H), 7.88–7.91 (m, 2H), 8.22–8.28 (m, 6H), 8.34 (d, J = 8 Hz, 2H), 8.38 (d, J = 4 Hz, 2H), 8.43 (d, J = 8 Hz, 2H), 8.28–8.32 (m, 2H); ^{13}C NMR

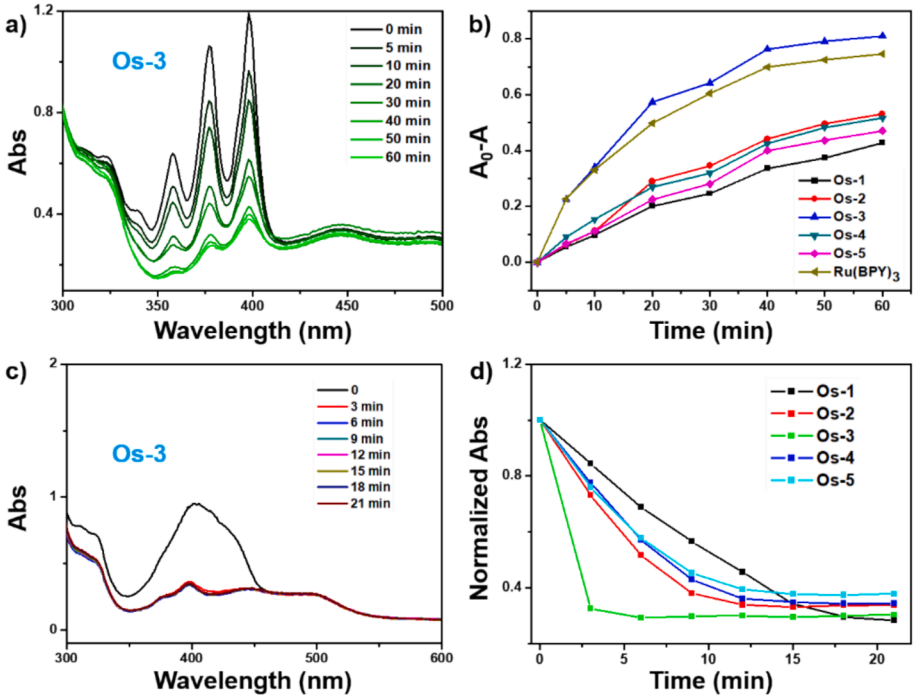

Fig. 3. A)the time-dependent absorption spectra of abda (60 μM) in the presence of Os-3 (10 μM) in acetonitrile under blue light irradiation (13 mW/cm^2) in 60 min; b)Absorbance change at 398 nm of Os-1 − Os-5 in comparison to Ru(bpy)$_3$ Cl$_2$; c) The time-dependent absorption of DPBF (40 μM) in the presence of Os-3 (10 μM) in acetonitrile under red light irradiation (40 mW/cm^2); d) Absorbance change at 415 nm of Os-1 − Os-5. (For interpretation of the references to colour in this figure legend, the reader is referred to the web version of this article.)

(100 MHz, $CDCl_3$) δ_C 152.9, 152.2, 151.5, 151.4, 150.1, 149.9, 149.8, 149.1, 148.8, 145.8, 141.9, 139.5, 139.2, 134.8, 130.6, 130.0, 129.9, 129.8, 129.5, 128.9, 128.8, 128.1, 128.0, 127.6, 126.8, 126.3, 126.2 HRMS-$[M]^{2+}$ Found: 645.1890 *m/z*, calculated: 645.1887 *m/z*. Anal. Calcd for $[C_{78}H_{50}F_{12}N_8OsP_2(H_2O)_{1.2}]$: C, 58.51; H, 3.30; N, 7.00. Found: C, 58.53; H, 3.50; N, 6.91.

Os-5 [(DIP)$_2$Os(dppzn)](PF$_6$)$_2$. Yield: 383 mg, 65 %. ^{1}H NMR (400 MHz, $CDCl_3$) δ 7. 23 (d, J = 8 Hz, 2H), 7.49–7.67 (m, 26H), 7.75–7.81 (m, 8H), 7.93–8.04 (m, 5H), 8.22–8.29 (m, 4H), 8.33 (s, 2H), 8.40 (s, 3H), 8.50 (d, J = 8 Hz, 2H), 9.44 (s, 2H); ^{13}C NMR (100 MHz, $CDCl_3$) δ_C 153.0, 152.3, 151.6, 151.5, 150.1, 150.0, 149.8, 149.1, 148.8, 145.8, 142.0, 139.6, 136.9, 134.8, 133.0, 130.6, 129.9, 129.8, 129.5, 128.9, 128.8, 128.7, 128.1, 127.9, 127.4, 127.2, 126.9, 126.4, 126.0; HRMS-$[M]^{2+}$ Found: 695.2040 *m/z*, calculated: 695.2043 *m/z*. Anal. Calcd for $[C_{86}H_{54}F_{12}N_8OsP_2(H_2O)_{1.8}]$: C, 60.33; H, 3.40; N, 6.55. Found: C, 60.33; H, 3.60; N, 6.61.

3.2. Electrochemical study

Cyclic voltammetry (CV) and differential pulse voltammetry (DPV) of **Os-1** — **Os-5** were performed using a CHI-730D electrochemistry workstation based on a reported procedure [40]. The workstation consists of a three-electrode-compartment cell: glass carbon electrode (Φ = 3 mm) served as the working electrode, while platinum wire and Ag/AgCl electrodes were used as the counter and reference electrodes, respectively, with tetrabutyl ammonium perchlorate (TBAP) as a supporting electrolyte, and *o*-dichlorobenzene (*o*-DCB) was used as the solvent.

3.3. Density functional theory calculations and time-dependent DFT calculations

Density functional theory (DFT) and TD-DFT calculations were performed with the Gaussian 09 program package [41]. The frontier molecular orbital and energy levels of **Os-1** — **Os-5** were calculated at the B3LYP/6-31G(d,p) (C, N, H) + SDD (Os) basis set.

3.4. Partition coefficient (Log P) determination

Solutions of Octanol-saturated water (OSW) and water-saturated octanol (WSO), were prepared by mixing analytical grade octanol and aqueous solution. Aliquots of osmium solutions of **Os-1** — **Os-5** in OSW were added to equal volumes of WSO and shaken for 24 h. The aqueous and octanol layers were subsequently separated into different tubes, and the absorbance of each solution was analyzed by UV–vis spectroscopy. Partition coefficient was calculated by the following equation:

$$\log P_{O/W} = \log\left([Os]_{WSO}/[Os]_{OSW}\right)$$

3.5. Singlet oxygen determination

Indirect method 1:

1,3-Diphenylisobenzofuran (DPBF) was dissolved in acetonitrile and diluted to give a final concentration of 60 μM and kept in the dark. Os(II) complexes in acetonitrile at a concentration of 20 μM were also prepared. After mixing 2 mL of DPBF solution with Os(II) complex suspension, curves and the absorbance at 415 nm were recorded every 3 min under red light (640 nm, 40 mW/cm^2) on a UV − vis spectrometer.

Indirect method 2 ($^1O_2$ quantum yield included):

Acetonitrile solutions of **Os-1 – Os-5** (20 μM) and 9,10-anthracenediyl-bis-(methylene) dimalonic acid (ABDA, 100 μM) were prepared in the dark and mixed. Mixtures were measured using UV–vis spectrophotometer after different blue light (465 nm, 13 mW/cm^2) irradiation durations. The absorbance changes of ABDA at 378 nm were also recorded, [Ru(bpy)$_3$Cl$_2$] was used as standard photosensitizer to quantify the quantum yields ($\Phi_{\Delta S}$) of $^1O_2$. Singlet oxygen generation yield was calculated by the following formula [42]:

$\Phi_{\Delta(S)} = \Phi_{\Delta(S0)} \times (Ss/Ss_0) \times 100$ %.

$\Phi_{\Delta(S)}$ = yield of Os(II) complexes, $\Phi_{\Delta(S0)}$ = yield of Ru(bpy)$_3$Cl$_2$,

Ss = slope of compounds, Ss_0 = slope of Ru(bpy)$_3$Cl$_2$.

Table 1
Half inhibition concentration (IC_{50}) values of Os-1 − Os-5 in the dark, upon irradiation at 640 nm (red light) and 465 nm (blue light) against A549, MGC-803 and HGC-27 cancer cell lines. Values are average of three independent tests.

Complex	cancer cell lines	dark	640 nm	PI-1	564 nm	PI-2
Os-1	A549	9.45 ± 1.60	8.51 ± 0.83	1.1	4.85 ± 0.34	1.9
	MGC-803	1.17 ± 0.12	0.39 ± 0.05	3	0.37 ± 0.03	3.2
	HGC-27	0.87 ± 0.15	0.32 ± 0.02	2.7	0.38 ± 0.04	2.3
Os-2	A549	89.21 ± 6.5	39.31 ± 4.71	2.3	5.89 ± 0.61	15
	MGC-803	1.20 ± 0.12	0.56 ± 0.04	2.1	0.39 ± 0.04	3.1
	HGC-27	1.00 ± 0.20	0.49 ± 0.05	2	0.39 ± 0.03	2.6
Os-3	A549	26.17 ± 1.87	20.41 ± 2.25	1.3	7.39 ± 1.61	3.5
	MGC-803	1.26 ± 0.28	0.79 ± 0.06	1.6	0.47 ± 0.03	2.7
	HGC-27	1.97 ± 0.16	1.20 ± 0.12	1.6	0.81 ± 0.06	2.4
Os-4	A549	10.67 ± 1.42	15.26 ± 1.73	n. d.	13.62 ± 1.34	n. d.
	MGC-803	1.14 ± 0.06	0.85 ± 0.04	1.3	0.68 ± 0.04	1.7
	HGC-27	0.94 ± 0.28	0.95 ± 0.25	n. d.	0.56 ± 0.17	1.7
Os-5	A549	8.90 ± 0.96	6.08 ± 0.82	1.5	4.43 ± 0.61	2
	MGC-803	2.19 ± 0.21	2.20 ± 0.15	n. d.	1.09 ± 0.06	2
	HGC-27	3.10 ± 0.28	3.02 ± 0.15	1	1.09 ± 0.14	2.8

PI = Phototherapeutic index, defined as [IC_{50}]dark / [IC_{50}]light; n.d. = not determined.

3.6. Antiproliferative activity by CCK-8 assay

The antiproliferative activity of **Os-1** − **Os-5** was studied by the CCK-8 assay. In general, exponentially grow cancer cells (1×10^5 cells per well) were seeded in a 96-well plate. After 24 h incubation for attachment, cells were incubated with different concentrations of Os(II) complexes from a stock solution (10 mM in DMSO), *i.e.*, 100, 50, 25, 12.5, 6.25, 3.13, 1.56, 0.78, 0.39, and 0.19 μM, for 12 h. Supernatant was then replaced with fresh culture medium and cells were subjected to LED light irradiation at 465 nm (blue LED light) or 640 nm (red LED light) for 1 h, and incubated for an additional 24 h. Cells without irradiation were replaced with fresh culture medium and maintained in the dark as control. Then 10 μL of CCK-8 (Adamas Life) working solution was added and incubated for another 1 h. Absorbance at 450 nm was measured on an TECAN (Infinite M Nano) microplate reader. Data were reported as the mean ± standard deviation (n = 3). The relative IC_{50} values of **Os-1** − **Os-5** were determined by plotting the percentage of viability versus concentration on a logarithmic graph.

3.7. Cellular uptake

Cells were seeded at a density of 5×10^6 in a 10 cm cell culture dish, and were administered with 10 μM of complexes **Os-1** and **Os-3** from a stock solution of 10 mM in DMSO, and the mixture was co-incubated for another 4 h. The medium was then removed; and cells were trypsinized, harvested, centrifuged, resuspended in PBS, and countered. Next,

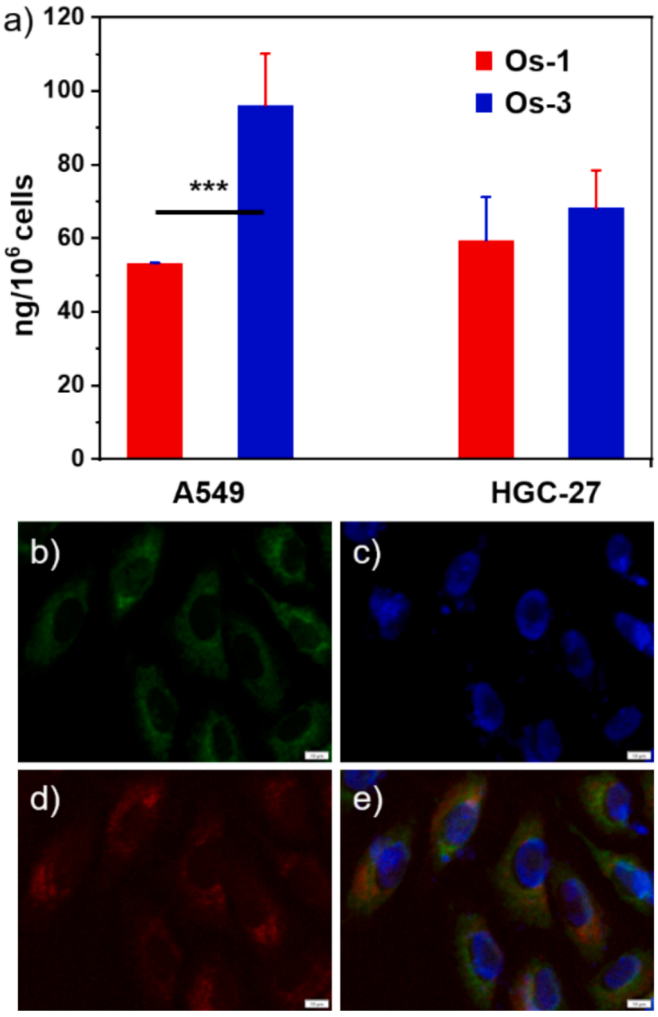

Fig. 4. a) Cellular uptake of Os-1 and Os-3 in A549 and HGC-27 cells measured by ICP-MS; Statistical significance was calculated with two-tailed Student's *t*-test, (*$p < 0.05$, **$p < 0.01$ or ***$p < 0.001$), all the experiments were performed as duplicates of triplicates; b) Mitochondria-localized dye MitoTracker Green (ex: 488 nm, em: 513–550 nm); c) Nucleus-specific dye Hoechst 33,342 (ex: 405 nm, em: 409–448 nm); d) Luminescence of Os-3; e) Merged image. (For interpretation of the references to colour in this figure legend, the reader is referred to the web version of this article.)

samples were digested with 70 % nitric acid (1 mL, 60 °C, 16 h) and then diluted in 1: 100 (1 % HCl solution in MQ water) before analyzing on ICP-MS. The Os isotopes at 188, 189, and 190 were monitored. The cellular uptake of Os was associated with the number of cells.

3.8. In-cell $^1O_2$ detection

HGC-27 cancer cells were incubated with different concentrations of **Os-3** (0.1, 1, and 2.5 μM) from a stock solution of 1 mM in DMSO for 8 h, and subsequently co-administered with the green fluorescent probe SOSG (2.5 μM, in DMSO) for 30 min. Next, the supernatant was removed and cancer cells were washed with PBS buffer 3 times. After that, cells were exposed to blue LED irradiation (465 nm, 13 mW/cm^2) for 1 h, and the green fluorescence was instantly observed on an OLYMPUS fluorescence microscope (CKX53, excitation wavelength, 488 nm; emission wavelength, 495–555 nm), cells treated with **Os-3** in the dark were set as positive control, cell with SOSG only was set as negative control.

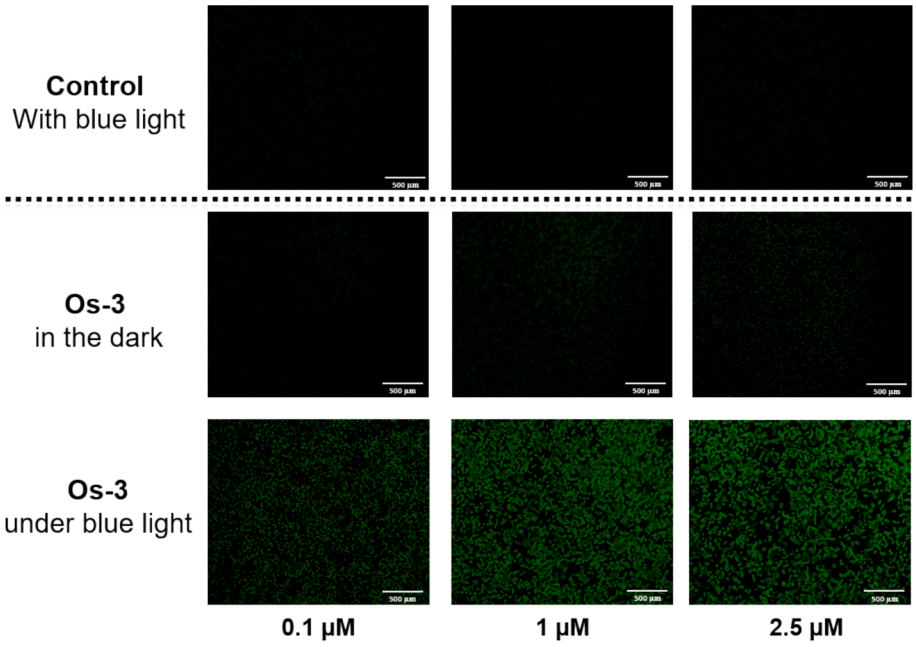

Fig. 5. In-cell singlet oxygen investigation with Os-3 using SOSG as the fluorescent probe by fluorescence microscope (excited at 488 nm; emission at 495–555 nm).

3.9. Subcellular localization by confocal microscopy

A549 cells were seeded and incubated in confocal dishes overnight at 37 °C (5 % CO_2). The next day, a solution (5 μ M, in DMSO) of complex **Os-3** was added to replace cell medium, and complex was incubated with cancer cells in the dark for 4 h. Next, the MitoTracker Green dye in DMSO was added at a final concentration of 75 nM, and a Hoechst 33,342 solution (in DMSO) was added to the dishes after 20 min. Cells were washed with PBS and imaged on an OLYMPUS SpinSR confocal microscope.

4. Results and discussion

4.1. Synthesis and characterization

The synthesis of Os(II) complexes **Os-1** — **Os-5** was based on the previous method [24], as shown in Scheme 1, all five complexes were fully characterized by ^{1}H and ^{13}C NMR, HRMS and elemental analysis (Figs. S1–S15). The octanol/water partition coefficients (log $P_{O/W}$) of **Os-1** — **Os-5** were also assessed, giving log *P* values of 1.11 (**Os-1**), 1.48 (**Os-2**), 0.64 (**Os-3**), 1.26 (**Os-4**), and 0.81 (**Os-5**).

The UV–vis spectra of complexes **Os-1** — **Os-5** in both acetonitrile and cell culture medium (1 % DMSO contained) were determined, which showed a typical panchromatic absorption in the wavelength range of 240 nm to *ca.* 760 nm; all five Os(II) complexes gave a similar absorption feature which are analogous to the Os(II) complex profiles reported by Gasser and Chao *et al.*[24]; As shown in Fig. 1 and Fig. S16, major and intense peaks at *ca.* 280 nm, that are assignable to the IL ππ* transitions of DIP were observed, while the adjacent two broad peaks at *ca.* 450 and 500 nm can be attributed to the metal to ligand charge transfer (MLCT) of Os(dπ) toward the chelated ligands(π*), and finally a weaker broadband covering the region 650–760 nm [43]. The latter can be explained by the spin-forbidden MLCT transitions due to the direct singlet–triplet transition of the Os(II) complexes [23,44]; which can be explained by the strong spin–orbit coupling of osmium, that often encountered in heavy atoms [24].

4.2. Electrochemical study

In order to further understand the electronic structure of **Os-1** to **Os-5**, the electrochemical characterizations were performed in *o*-dichlorobenzene (*o*-DCB) solutions containing 2 mM **Os-1** to **Os-5** and 0.1 M TBAP as the supporting electrolytes (Fig. S17 and Fig. S18). The investigated five complexes **Os-1** to **Os-5** exhibit multi-redox potential peaks, indicates the powerful multi-electron donating and accepting properties as a result of its larger molecular skeleton (Table S1) [45]. Cyclic voltammetry of **Os-1** — **Os-5** (Fig. S17 and Table S1) exhibited the oxidation processes in the range of + 0.97 V — +1.19 V, which are assignable to the Os(II/III) couples, this is probably due to the powerful electron-withdrawing property of DIP ligand [46]; while the reductive electrochemistry of **Os-1** — **Os5** was more complicated, the most anodic process for those Os(II) complexes, that centered at −0.38 V — -0.76 V, were assigned to the DIP based reduction process, the second and third reduction waves are assigned to the coordinative ligands **L1-L5** [46,47]. The 1st Red.-1st Ox. gaps of **Os-1** to **Os-5** are 1.76, 1.54, 1.93, 1.73, and 1.71 eV, respectively.

4.3. DFT calculations and TD-DFT calculations

DFT calculations for five complexes were performed to better investigate the electronic property (Fig. 2). In general, **Os-1** — **Os-5** showed a HOMO-LUMO gap in the range of 2.19–3.41 eV. For complexes **Os-3** — **Os-5**, the lowest unoccupied molecular orbital (LUMO) is mainly constituted of π* phenanthroline ligand orbitals, while the highest occupied molecular orbital (HOMO) resides almost exclusively on the aromatic substituents (phenyls for **Os-4**, and naphthalenes for **Os-5**), the electron distributions are contrary to that of complexes **Os-1** and **Os-2**. The attachment of aromatic rings led to a gentle orbital stabilization of 0.3–0.5 eV for complexes **Os-3** — **Os-5**, leaving the LUMO energy (approx. 6.45 eV) barely perturbed. Hence, such distribution may demonstrate an apparent intramolecular charge transform (ICT) absorption for these complexes [48]. Next, time-dependent DFT (TD-DFT) calculations were also performed. The simulated electronic absorption spectra were depicted in Figs. S19–S23 and Tables S2–S6. The frontier molecular orbitals and TD-DFT result of **Os-1-Os-5** exhibited the absorption of main bands are all assignable to UV–vis absorptions, with the highest oscillator strengths (*f*) of **Os-1-Os-5** in the range of 0.2 to 0.4. The DFT and TD-DFT results further confirmed the ICT transform absorptions for **Os-1-Os-5**.

4.4. $^1O_2$ generation

Initially, the photo-stability of these Os(II) complexes was determined under blue LED light irradiation (Fig. S24), all Os(II) complexes showed high photo-stability in 60 min under irradiation. Next, the singlet oxygen generation capacity of complexes **Os-1** — **Os-5** was determined using ABDA as a trapping agent, and Os (II) complexes with ABDA in the dark was set as negative control (Fig. S25). As shown in Fig. 3. and Fig. S26, ABDA can be degraded by all Os (II) complexes in 60 min under blue LED light irradiation (465 nm); as shown in Fig. 3b, the conjugative π extension of coordinative ligands from L1 to L3 has given an pronounced enhancement in the $^1O_2$ generation rate for **Os-1** — **Os-3**, in the order of **Os-1** < **Os-2** < **Os-3**, complex **Os-3** gave the highest efficiency that oxidized ABDA in 30 min which is comparable to $Ru(bpy)_3Cl_2$, however, the π extensions by covalent bonding for **Os-4** and **Os-5** have rarely changed the generation rate in comparison to **Os-2**. The $^1O_2$ quantum yield of five Os (II) complexes were in the range of 0.36–0.65 (Fig. S26 and Table S7), where **Os-3** with a quantum yield value of 0.65, is apparently higher than $Ru(bpy)_3Cl_2$ (0.57 in ACN), and is higher than those of Os(II) complexes by Gilles *et al.* [24]. $^1O_2$ generation in aqueous solutions by **Os-1** — **Os-5** was also determined with the same method above to investigate the influence of aqua (DMSO/H_2O, 1:9) on the quantum yield, as shown in Fig. S27 and Table S7, the $^1O_2$ quantum yields of **Os-1** — **Os-5** were significantly lower with quantum yield values in the range of 0.14–0.27.

Next, the $^1O_2$ generation by the Os (II) complexes were also investigated under red LED irradiation (640 nm) with DPBF as the trapping agent, Os (II) complexes with DPBF in the dark was also set as negative control (Fig. S28); all complexes showed a similar efficiency trend to that of blue LED light irradiation, **Os-3** remained the most pronounced $^1O_2$ generation ability among five Os(II) complexes that the inductively generated $^1O_2$ by **Os-3** can decompose DPBF within 1 min (Fig. 3c and d, Fig. S29, and Fig. S30). The conjugative π-ring elongation from **Os-1** to **Os-3** have improved the rigidity of the molecules, thus may have diminished the vibrational relaxation rate of energy transfer, that resulted into an apparent enhancement of $^1O_2$ generation [29].

4.5. Antiproliferative activity in vitro

Anticancer activity of five Os(II) complexes against three cancerous cell lines, A549 human non-small cell lung cancer, MGC-803, and HGC-27 (undifferentiated) human gastric cancer cells was determined with two LED light irradiations: 640 nm (red LED light) and 465 nm (blue LED light), and compared with the control group (in the dark), cisplatin and 5-ALA were investigated as positive control. As shown in Table 1, **Os-1** — **Os-5** showed low cytotoxicity towards A549 cells, with most of the IC_{50} values over 10 μM in the dark. Gratifyingly, **Os-2** induced a significant photocytotoxicity against A549 cells under blue LED light irradiation, with PI value as high as 15, while for the rest of the PI values are all lower than 5. Of note, all Os(II) complexes could induce an potent cell viability deduction against human gastric cancer cells, i.e. MGC-803 and HGC-27 cell lines, with IC_{50} values in the range of 0.32 to 2.2 μM, the major of which are nanomolar levels. While regretfully, all complexes showed obvious cytotoxicity against gastric cancer cells even in the dark, with the IC_{50} values fell within the scope of 0.87–3.10 μM, which were much more cytotoxic than that of cisplatin and 5-ALA as shown in Table S8. **Os-1** — **Os-5** also showed an apparent growth inhibition on all tested cancer cells under red LED light irradiation, the IC_{50} value was low as 0.32 μM (PI = 2.7). The significant inhibition of cell viability in MGC-803 and HGC-27 cells under blue light irradiation, confirmed the potential application of these Os(II) complexes as promising photosensitizers and chemotherapeutic drugs in treatment of gastric cancers.

4.6. Cellular uptake

The cell uptake of complexes **Os-1** and **Os-3** was determined in A549 and HGC-27 cancer cells using inductively coupled plasma mass spectrometry (ICP-MS). As shown Fig. 4 and Table S9. **Os-3** in A549 cells was found to have the highest cellular uptake of 96.1 ng/10^6 cells; and have 68.2 ng/10^6 cells in HGC-27 cells after 4 h co-incubation; these are higher than that of **Os-1** in the A549 and HGC-27 cells, which were *ca.* 55 ng per 10^6 cells (53.3 vs 59.4), respectively; this is probably due to the higher lipophilicity of ligand L3 in comparison to L1.

4.7. Subcellular localization and in cell $^1O_2$ determination

The subcellular localization of **Os-3** in A549 human non-small cell lung cancer cells was determined by confocal microscopy using Hoechst33342 (nucleus) and MitoTracker Green (MTG, mitochondrial) as tracking dyes (Fig. 4b). The luminescence of **Os-3** was appeared as a diffused signal in A549 cells after 4 h incubation (Fig. 4d), and showed weak signal overlap with MTG, suggested that **Os-3** has a low tendency to target mitochondria. While only limited accumulation of **Os-3** in the nucleus, as shown by the absence of colocalization with Hoechst 33,342 and MitoTracker Green (Fig. 4c and 4e).

Next, the in-cell $^1O_2$ generation by **Os-3** under the concentrations of 0.1, 1 and 2.5 μM, was investigated in HGC-27 human gastric cancer cells, using SOSG as the green fluorescent sensor, cells with SOSG only were applied as negative control. As shown in Fig. 5, the fluorescence signals in cells by three different concentrations of **Os-3** were observed, and exhibited a concentration-dependent manner, that the intensity has been enhanced when co-administered with 2.5 μM of **Os-3** under blue LED light irradiation, while only weak fluorescence signals in HGC-27 cells with **Os-3** were seen in the dark. The different observed fluorescence signals demonstrated the PDT mechanism of action of such Os(II) complexes in cancer cells.

5. Conclusions

In summary, we have designed and synthesized five polypyridyl Os (II) complexes **Os-1** — **Os-5**, these complexes were fully characterized by NMR, HRMS and elemental analysis; **Os-1** — **Os-5** showed a panchromatic UV–vis absorption character. The electronic properties of **Os-1** — **Os-5** were investigated by CV and DFT calculations. An obvious $^1O_2$ generation enhancement tendency was observed when π ring of the coordinative ligand was conjugatively elongated, led to a rising order of **Os-1** < **Os-2** < **Os-3** under either blue or red LED irradiation, and the $^1O_2$ quantum yield ($\Phi_{\Delta S}$) of **Os-3** was even higher than the reference complex $Ru(bpy)_3Cl_2$ (0.65 VS 0.57), however the covalent π ring bond for **Os-4** and **Os-5** did not facilitate further $^1O_2$ generation in comparison to that of the parent structure-**Os-2**. **Os-1** — **Os-5** exhibited potent antiproliferative activity against MGC-803 and HGC-27 human gastric cancer cells, with IC_{50} values low as 0.37 μM (blue LED light) and 0.32 μM (blue LED light), **Os-2** gave the highest PI value (PI = 15) in A549 cancer cell inhibition. Cell uptake of **Os-1** and **Os-3** in A549 and HGC-27 cells was in the range of 53–96 ng/10^6 cells. In cell $^1O_2$ detection displayed a concentration-dependent manner, and the complex was not accumulated in nucleus, nor targeting mitochondria upon entering cells. The trend in $^1O_2$ generation of these Os(II) complexes may provide a useful strategy for the development of photosensitizers, and the potent anticancer activity of **Os-1** — **Os-5** may demonstrate a potential application in PDT and chemotherapeutic therapy in gastric cancer treatment.

CRediT authorship contribution statement

Feng Chen: Data curation, Formal analysis, Funding acquisition, Methodology, Project administration, Writing – review & editing. **Kelun Cui:** Formal analysis, Investigation, Writing – review & editing. **Shufen**

Si: Data curation, Methodology, Resources, Validation. **Yong Liu:** Investigation, Methodology. **Songlin Xue:** Funding acquisition, Investigation, Methodology, Writing – original draft. **Gaoji Wang:** Funding acquisition, Investigation, Project administration, Writing – original draft, Writing – review & editing. **Xu Liang:** Methodology, Project administration, Writing – original draft, Writing – review & editing. **Chunyin Zhu:** Project administration, Supervision, Writing – review & editing. **Qiu-Yun Chen:** Methodology, Project administration, Supervision, Writing – original draft, Writing – review & editing.

Declaration of competing interest

The authors declare that they have no known competing financial interests or personal relationships that could have appeared to influence the work reported in this paper.

Acknowledgements

This work was partly supported by the National Natural Science Foundation of China (Grant No. 22207046 and 22301108), Natural Science Foundation of Jiangsu Province (Grant No. BK20220528), and the Project Startup Foundation for Distinguished Scholars of Jiangsu University (4111310026, 5501310019, and 5501310014).

Appendix A. Supplementary data

Supplementary data to this article can be found online at https://doi.org/10.1016/j.ica.2025.122537.

Data availability

Data will be made available on request.

References

[1] X. Wang, X. Wang, S. Jin, N. Muhammad, Z. Guo, Chem. Rev. 119 (2019) 1138–1192.
[2] B.S. Murray, M.V. Babak, C.G. Hartinger, P.J. Dyson, Coord. Chem. Rev. 306 (2016) 86–114.
[3] S. Thota, D.A. Rodrigues, D.C. Crans, E.J. Barreiro, J. Med. Chem. 61 (2018) 5805–5821.
[4] Z. Liu, P.J. Sadler, Acc. Chem. Res. 47 (2014) 1174–1185.
[5] L. Wang, R. Guan, L. Xie, X. Liao, K. Xiong, T.W. Rees, Y. Chen, L. Ji, H. Chao, Angew. Chem. Int. Ed. 60 (2021) 4657–4665.
[6] S. Kuang, F. Wei, J. Karges, L. Ke, K. Xiong, X. Liao, G. Gasser, L. Ji, H. Chao, J. Am. Chem. Soc. 144 (2022) 4091–4101.
[7] S.C. Marker, A.P. King, R.V. Swanda, B. Vaughn, E. Boros, S.-B. Qian, J.J. Wilson, Angew. Chem. Int. Ed. 59 (2020) 13391–13400.
[8] S.C. Marker, A.P. King, S. Granja, B. Vaughn, J.J. Woods, E. Boros, J.J. Wilson, Inorg. Chem. 59 (2020) 10285–10303.
[9] J. Jiang, B. Cao, Y. Chen, H. Luo, J. Xue, X. Xiong, T. Zou, Angew. Chem. Int. Ed. 61 (2022) e202201103.
[10] J. Karges, Angew. Chem. Int. Ed. 61 (2022) e202112236.
[11] C.-P. Tan, Y.-M. Zhong, L.-N. Ji, Z.-W. Mao, Chem. Sci. 12 (2021) 2357–2367.
[12] S. Monro, K.L. Colon, H. Yin, J. Roque, P. Konda, S. Gujar, R.P. Thummel, L. Lilge, C.G. Cameron, S.A. McFarland, Chem. Rev. 119 (2019) 797–828.
[13] S.A. McFarland, A. Mandel, R. Dumoulin-White, G. Gasser, Curr. Opin. Chem. Biol. 56 (2020) 23–27.
[14] C. Marie, V. Pierroz, S. Ferrari, G. Gasser, Chem. Sci. 6 (2015) 2660–2686.
[15] F. Heinemann, J. Karges, G. Gasser, Acc. Chem. Res. 50 (2017) 2727–2736.
[16] P. Ogilby, Chem. Soc. Rev. 39 (2010) 3181–3209.
[17] Y. Zhang, B.-T. Doan, G. Gasser, Chem. Rev. 123 (2023) 10135–10155.
[18] R.G. Kenny, C.J. Marmion, Chem. Rev. 119 (2019) 1058–1137.
[19] L. Conti, E. Macedi, C. Giorgi, B. Valtancoli, V. Fusi, Coord. Chem. Rev. 469 (2022) 214656.
[20] A. Hernández-García, L. Marková, M.D. Santana, J. Pracharová, D. Bautista, H. Kostrhunová, V. Novohradsky,· V. Brabec, J. Ruiz, and J. Kasˇpárková, Inorg. Chem. 62 (2023) 6474–6487.
[21] M.-F. Wang, Y.-A. Deng, Q.-F. Li, S.-J. Tang, R. Yang, R.-Y. Zhao, F.-D. Liu, X. Ren, D. Zhang, F. Gao, Chem. Commun. 58 (2022) 12676–12679.
[22] J.A. Roque III, P.C. Barrett, H.D. Cole, L.M. Lifshits, G. Shi, S. Monro, D. von Dohlen, S. Kim, N. Russo, G. Deep, C.G. Cameron, M.E. Alberto, S.A. McFarland, Chem. Sci. 11 (2020) 9784–9806.
[23] S. Lazic, P. Kaspler, G. Shi, S. Monro, T. Sainuddin, S. Forward, K. Kasimova, R. Hennigar, A. Mandel, S. McFarland, L. Lilge, Photochem. Photobiol. 93 (2017) 1248–1258.
[24] A. Mani, T. Feng, A. Gandioso, R. Vinck, A. Notaro, L. Gourdon, P. Burckel, B. Saubaméa, O. Blacque, K. Cariou, J.-E. Belgaied, H. Chao, G. Gasser, Angew. Chem. Int. Ed. 62 (2023) e202218347.
[25] N. Lu, Z. Deng, J. Gao, C. Liang, H. Xia, P. Zhang, Nat. Commun. 13 (2022) 2245.
[26] P. Zhang, Y. Wang, K. Qiu, Z. Zhao, R. Hu, C. He, Q. Zhang, H. Chao, Chem. Commun. 53 (2017) 12341–12344.
[27] J.J. Nogueira, M. Oppel, L. Gonźlez, Angew. Chem. Int. Ed. 54 (2015) 4375–4378.
[28] J. Zhao, Y. Gao, R. Huang, C. Chi, Y. Sun, G. Xu, X.-Hua Xia, and S. Gou, J. Am. Chem. Soc. 145 (2023) 11633–11642.
[29] J.A. Treadway, B. Loeb, R. Lopez, P.A. Anderson, F.R. Keene, T.J. Meyer, Inorg. Chem. 35 (1996) 2242–2246.
[30] K.M. Kuznetsov, K. Cariou, G. Gasser, Chem. Sci. 15 (2024), https://doi.org/10.1039/d4sc04608k.
[31] N. Macia, V. Kabanov, B. Heyne, J. Phys. Chem. C 124 (2020) 3768–3777.
[32] M.R. Younis, R. An, Y. Wang, G. He, B. Gurram, S. Wang, J. Lin, D. Ye, P. Huang, X.-H. Xia, ACS Appl. Bio Mater. 5 (2022) 747–760.
[33] S. Mishra, S.B. Shelar, S. Rout, P.A. Hassan, K.C. Barick, N. Agarwal, ACS Appl. Bio Mater. 7 (2024), https://doi.org/10.1021/acsabm.4c00804.
[34] X. Nie, S. Wu, A. Mensah, Q. Wang, F. Huang, Q. Wei, Chem. Eng. J. 395 (2020) 125012.
[35] Z. Molphy, A. Prisecaru, C. Slator, N. Barron, M. McCann, J. Colleran, D. Chandran, N. Gathergood, A. Kellett, Inorg. Chem. 53 (2014) 5392–5404.
[36] A.J. McConnell, M.H. Lim, E.D. Olmon, H. Song, E.E. Dervan, J.K. Barton, Inorg. Chem. 51 (2012) 12511–12520.
[37] S.K. Chandy, S.A. Bowers, M. Yin, L. Liu, K. Raghavachari, L. Li, Inorg. Chem. 61 (2022) 17505–17514.
[38] B. Schäfer, H. Görls, M. Presselt, M. Schmitt, J. Popp, W. Henry, J.G. Vosc, S. Rau, Dalton Trans. 18 (2006) 2225–2231.
[39] E.M. Kober, J.V. Caspar, B.P. Sullivan, T.J. Meyer, Inorg. Chem. 27 (1988) 4587–4598.
[40] X. Zhang, X. Zhang, W. Zhu, X. Liang, Dalton Trans. 51 (2022) 6177–6185.
[41] Gaussian 09, Revision B.01, M. J. Frisch, G. W. Trucks, H. B. Schle-gel, G. E. Scuseria, M. A. Robb, J. R. Cheeseman, G. Scalmani, V. Barone, B. Mennucci, G. A. Petersson, H. Nakatsuji, M. Caricato, X. Li, H. P. Hratchian, A. F. Izmaylov, J. Bloino, G. Zheng, J. L. Son-nenberg, M. Hada, M. Ehara, K. Toyota, R. Fukuda, J. Hasegawa, M. Ishida, T. Nakajima, Y. Honda, O. Kitao, H. Nakai, T. Vreven, J. A. Montgomery, Jr., J. E. Peralta, F. Ogliaro, M. Bearpark, J. J. Heyd, E. Brothers, K. N. Kudin, V. N. Staroverov, T. Keith, R. Kobayashi, J. Normand, K. Raghavachari, A. Rendell, J. C. Burant, S. S. Iyengar, J. Tomasi, M. Cossi, N. Rega, J. M. Millam, M. Klene, J. E. Knox, J. B. Cross, V. Bakken, C. Adamo, J. Jaramillo, R. Gomperts, R. E. Strat-mann, O. Yazyev, A. J. Austin, R. Cammi, C. Pomelli, J. W. Ochter-ski, R. L. Martin, K. Morokuma, V. G. Zakrzewski, G. A. Voth, P. Salvador, J. J. Dannenberg, S. Dapprich, A. D. Daniels, O. Farkas, J. B. Foresman, J. V. Ortiz, J. Cioslowski, and D. J. Fox, Gaussian, Inc., Wallingford CT, 2010.
[42] N. Manav, R. Singh, A. Janaagal, A.K.S. Yadav, V. Pandey, I. Gupta, New J. Chem. 46 (2022) 19310–19321.
[43] Y. Wei, M. Zheng, L. Chen, X. Zhou, S. Liu, Dalton Trans. 48 (2019) 11763–11771.
[44] E. Kianfar, D. Apaydin, G. Knör, ChemPhotoChem 1 (2017) 378–382.
[45] S. Xue, D. Kuzuhara, N. Aratani, H.Y amada, Org. Lett. 21 (2019) 2069.
[46] M. Stitch, R.Z. Boota, A.S. Chalkley, T.D. Keene, J.C. Simpson, P.A. Scattergood, P. I.P. Elliott, S.J. Quinn, Inorg. Chem. 61 (2022) 14947–14961.
[47] D. Graczyk, R.A. Cowin, D. Chekulaev, M.A. Haigh, P.A. Scattergood, S.J. Quinn, Inorg. Chem. 63 (2024) 23620–23629.
[48] S. Xue, N. Liu, P. Mei, D. Kuzuha, M. Zhou, J. Pan, H. Yamada, F. Qiu, Chem. Commun. 57 (2021) 12808–12811.